BIOCHEMISTRY
including biophysical chemistry & molecular biology

Article

pubs.acs.org/biochemistry

Impact of Reduced Rhodopsin Expression on the Structure of Rod Outer Segment Disc Membranes

Tatini Rakshit and Paul S.-H. Park*

Department of Ophthalmology and Visual Sciences, Case Western Reserve University, Cleveland, Ohio 44106, United States

ABSTRACT: Rhodopsin is the light receptor embedded in rod outer segment (ROS) disc membranes of photoreceptor cells that initiates vision via phototransduction. The relationship between rhodopsin expression and the formation of membrane structures in the ROS is unclear but important to better understand both normal function and pathological conditions. To determine the impact of reduced rhodopsin expression on the structure of ROS discs and the supramolecular organization of rhodopsin, ROS disc membrane samples from heterozygous rhodopsin knockout mice were examined by atomic force microscopy. Similar to rhodopsin in wild-type mice, rhodopsin formed nanodomains in ROS disc membranes of heterozygous knockout mice. The reduced rhodopsin expression in heterozygous knockout mice resulted in ROS disc membranes that were smaller compared to those in wild-type mice at all ages tested. Changes in ROS disc membrane properties were observed between 4 and 6 weeks of age in heterozygous knockout mice that were not present in age-matched wild-type mice. In 4 week old mice, the number and density of rhodopsin in ROS disc membranes was lower than that in age-matched wild-type mice. In contrast, 6 and 8 week old mice had more rhodopsin molecules present in disc membranes compared to 4 week old mice, which resulted in rhodopsin densities similar to those found in age-matched wild-type mice. Thus, mechanisms appear to be present that maintain a constant density of rhodopsin within ROS disc membranes even when reducing the expression of the light receptor by about half. These adaptive mechanisms, however, only occur after 4 weeks of age.

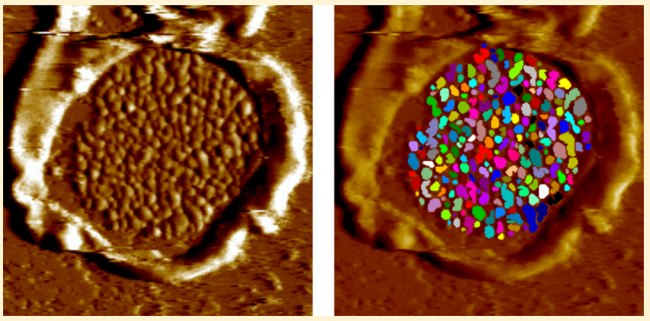

Rod photoreceptor cells are the most abundant cell type in the outer retina of most mammalian species. These photoreceptor cells are required for scotopic vision and are therefore tuned to achieve maximal sensitivity to light. Rhodopsin is the light receptor in rod photoreceptor cells and a prototypical G protein-coupled receptor that initiates vision upon photon capture. The receptor is embedded at high concentrations in rod outer segment (ROS) disc membranes of photoreceptor cells. The high concentrations of rhodopsin in disc membranes contribute to the high probability of photon capture. The ROS structure is formed by 500−2000 discs stacked one on top of another encased by a plasma membrane[1−3] (Figure 1). Discs are double lamellar membranes circumscribed by a rim region. The ROS is a dynamic structure with discs continuously formed at its base and displaced at its apical end via phagocytosis by retinal pigment epithelial cells.[4] Rhodopsin is by far the most abundant protein in the ROS, representing about 90% of all proteins in this compartment.[5] Rhodopsin has a key structural role in the ROS, since its absence prevents the formation of the ROS and results in photoreceptor cell death.[6,7]

Rhodopsin is synthesized in the inner segment of rod photoreceptor cells and is trafficked to the ROS and incorporated into discs via a multistep process[8−11] (Figure 1). The mechanisms underlying the incorporation of rhodopsin into the membrane of ROS discs and the achievement of a supramolecular membrane organization is still unclear. Atomic force microscopy (AFM) can provide much needed insights in these areas because it allows for the direct visualization of membrane proteins within the native environment of a lipid bilayer and physiological buffer conditions.[12−14] AFM has revealed that rhodopsin is organized into domains within ROS disc membranes that are composed of rows of dimeric receptor.[15−17] These domains are referred to as nanodomains since the dimensions are less than 100 nm.[17] Nanodomains formed by oligomeric rhodopsin likely represent the native organization of disc membranes since cryoelectron tomograms of disc membranes in a preserved intact ROS or a cryosectioned ROS exhibit densities that are consistent with such an organization.[2,18] This type of order may help facilitate the high sensitivity required from rod photoreceptor cells.[18,19]

AFM imaging and quantitative analysis of single ROS disc membranes are beginning to reveal some novel insights about ROS disc properties.[17] The diameter of discs in a ROS is not uniform but can range in size from 0.7−1.9 μm. Quantitative analyses using AFM data from single ROS disc membranes revealed a correlation between the size of a disc and the number of rhodopsin molecules incorporated into its membrane but no correlation between the size of a disc and the density at which rhodopsin is present in its membranes. Thus, the size of discs appears to be modulated in response to changes in the quantity of

Received: January 2, 2015
Revised: April 16, 2015
Published: April 17, 2015

DOI: 10.1021/acs.biochem.5b00003
Biochemistry 2015, 54, 2885−2894

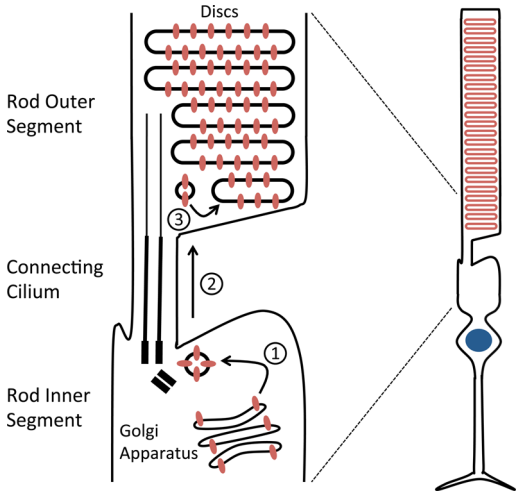

Figure 1. Schematic of a rod photoreceptor cell. The cartoon on the left shows a zoomed in view of a photoreceptor cell. Rhodopsin (red ellipses) is synthesized in the rod inner segment, transported to the base of the connecting cilium via post-Golgi vesicles (1), transported across the connecting cilium to the ROS (2), and incorporated into discs at the base of the ROS (3).

rhodopsin incorporated into the membrane to maintain a constant density of the receptor. These insights suggest that reducing the level of rhodopsin expression can have significant impact on the structure of ROS discs.

A reduction in the number of rhodopsin molecules available for incorporation into the membrane of ROS discs occurs in some cases of retinitis pigmentosa, a progressive neurodegenerative disease.[20,21] There are over 100 mutations in rhodopsin that cause retinitis pigmentosa.[21,22] A majority of mutations result in misfolded rhodopsin and cause an autosomal dominant form of the disease.[23,24] In these instances, the level of correctly folded rhodopsin available for incorporation into ROS disc membranes is severely reduced. Heterozygous rhodopsin knockout (Rho+/−) mice provide a model to study the impact of reduced rhodopsin expression on ROS and disc structure.[6,7] These mice have only one copy of the rhodopsin gene and express about half the amount of rhodopsin protein compared to wild-type mice.[6]

Electron microscopy studies have revealed that the size of the ROS is smaller in Rho+/− mice and discs can have altered shapes and more pronounced incisures.[25−27] Structural changes are accompanied by changes in the electrophysiological response of the ROS.[25,28] These studies provide a glimpse into the global changes occurring in the ROS in response to reduced rhodopsin expression; however, the picture is far from complete. For instance, the progression of these observed changes and the changes occurring in individual discs are unknown. There are also conflicting opinions on the impact of reduced rhodopsin expression on the density of the receptor present in disc membranes.[25,28] Thus, it is unclear how reduced rhodopsin expression impacts the packing of the receptor in the disc membrane. In the current study, AFM was utilized to directly visualize single ROS disc membranes and the nanodomain organization of rhodopsin to gain a better understanding of changes occurring in discs as a consequence of reducing the level of rhodopsin expression.

MATERIALS AND METHODS

ROS Disc Membrane Preparation. ROS disc membranes were prepared from the retinas of 9−15 C57Bl/6J mice (The Jackson Laboratory, Bar Harbor, ME) or Rho+/− mice.[6] Rhodopsin knockout mice were backcrossed with C57Bl/6J mice at least 10 generations and then mated with C57Bl/6J mice to generate Rho+/− mice. All procedures were conducted under dim red light conditions. Mice were dark-adapted overnight prior to being sacrificed. ROS disc membranes were obtained from murine retinas using procedures reported previously.[2,29] ROS disc membranes were resuspended in 50 μL of Ringer's buffer (10 mM HEPES, 130 mM NaCl, 3.6 mM KCl, 2.4 mM $MgCl_2$, 1.2 mM $CaCl_2$, 0.02 mM EDTA, pH 7.4). At least two preparations were examined for each age and mouse line tested except for 8 week old Rho+/− mice. Data obtained from different preparations of ROS disc membranes were similar. Previously, data from different preparations of ROS disc membranes from human and murine eyes were also shown to be similar.[17]

AFM Imaging. AFM generates topographical images of samples by raster-scanning a sharp probe across the surface of the sample. Different modes are available in commercial AFM instruments to capture topographical images (reviewed in refs 30 and 31). Each imaging mode can generate different types of images that contain distinct information about the scanned sample. Contact mode and tapping mode were utilized in the current study. Height, deflection, and amplitude images were

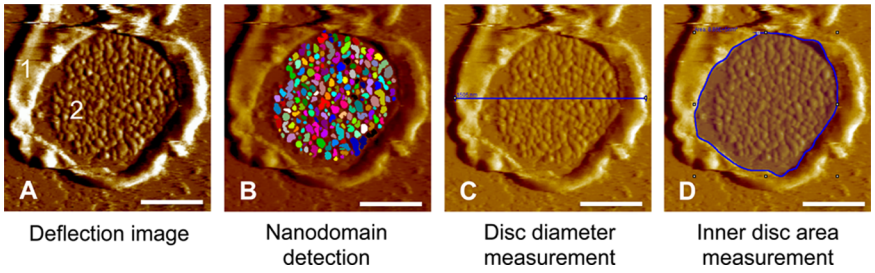

Figure 2. Analysis of AFM images. ROS disc membranes were isolated from mice, adsorbed on a mica substrate, and imaged by AFM. (A) The deflection image of a ROS disc membrane obtained by contact mode is shown. Two distinct topographical features are observed in the image: 1, rim region; 2, lamellar region. The deflection image was analyzed using the software SPIP (version 6.2, Image Metrology A/S) as described in the Materials and Methods to measure various parameters describing ROS disc membrane properties. (B) Nanodomains were detected by the software using a threshold-based method. Detected nanodomains in the deflection image are highlighted by randomly selected colors. The size of each nanodomain was computed by the software from the highlighted regions. (C) The disc diameter was measured by drawing a line along the longest axis. The length of the line was computed by the software. (D) The inner disc area was measured by highlighting the disc membrane area excluding the rim region. The area of the highlighted region was computed by the software. Scale bar, 500 nm.

DOI: 10.1021/acs.biochem.5b00003
Biochemistry 2015, 54, 2885−2894

collected. Height images contain information on the height of resolved features in images. Deflection and amplitude images accentuate the edges of resolved features in images but contain no height information.[30]

All AFM procedures were conducted at ambient temperatures under dim red light. ROS disc membrane samples were adsorbed on mica and prepared for AFM as described previously.[17,32] ROS disc membranes were imaged by AFM in imaging buffer (20 mM Tris, 150 mM KCl, 25 mM $MgCl_2$, pH 7.8). Contact mode AFM was performed using a Multimode II atomic force microscope equipped with an E scanner (Bruker Corporation, Santa Barbara, CA) as described previously.[17] NP-S and DNP-S cantilevers (Bruker Corporation, Santa Barbara, CA) with a nominal spring constant of 0.06 N/m were used. Samples were imaged at a scan rate of 5.09 Hz to acquire images at a resolution of 512 lines per frame. Height and deflection images were collected for analysis. Tapping mode AFM was performed using a 5500 atomic force microscope equipped with a 90 μm scanner (Keysight Technologies, Santa Rosa, CA). Images were obtained with DNP-S cantilevers (Bruker Corporation, Santa Barbara, CA) with a nominal spring constant of 0.24 N/m. Cantilevers were oscillated at 14−17 kHz and scanned at a speed of 0.85−1.42 lines/s to capture images at a resolution of 512 lines per frame. Height and amplitude images were collected for analysis.

AFM Image Analysis. AFM images were analyzed using the software SPIP (version 6.2, Image Metrology A/S, Hørsholm, Denmark). Lateral features of ROS disc membranes were analyzed from deflection or amplitude images (Figure 2A). The dimensions of nanodomains were measured semiautomatically using the Particle and Pore Analysis module. Nanodomains were detected using the Advanced Threshold detection method (Figure 2B). Nanodomains were detected as particles semiautomatically by adjusting the RMS Factor and Split Particles settings. The software determined the areas of detected nanodomains. The number of rhodopsin molecules in a nanodomain was estimated as done previously using the computed nanodomain area and assuming that rhodopsin forms oligomeric complexes.[17] The diameter of the disc membrane was measured using the Caliper Tool (Figure 2C). Since disc membranes often deviate from a perfect circle, the reported diameter is that of the longer axis. The inner disc area was determined using the Polygon Shape Tool to highlight the disc membrane area excluding the rim region (Figure 2D). The density of rhodopsin in a disc membrane was calculated by dividing the total number of rhodopsin molecules in a disc membrane by the inner disc area. Thus, the reported density values represent the rhodopsin density if single rhodopsin molecules were homogeneously organized in the membrane. The density of nanodomains in a disc membrane was calculated by dividing the number of nanodomains in a disc membrane by the inner disc area. Heights of nanodomains were determined from height images that were flattened in SPIP using a first order plane correction method and setting the background to zero. Nanodomains were detected using the Particle and Pore Analysis module as described above and the heights of the detected nanodomains were determined by the software. Statistical analyses were performed using Prism 6 (GraphPad Software, Inc., La Jolla, CA). Mean values are reported with the associated standard deviation. The n value is provided for each statistical analysis conducted and represents the number of AFM images of single ROS disc membranes used in the analysis.

RESULTS

Analysis of ROS Disc Membranes. AFM images of ROS disc membranes were previously analyzed manually.[17] To improve on the efficiency and accuracy of the previous analysis method, a semiautomated method was implemented in the current study. To directly compare the two analysis methods, previously reported data were reanalyzed.[17] ROS disc membranes adsorbed on a mica substrate display a distinct topography when imaged by AFM. Adsorbed membranes display a rim region, where rhodopsin is largely excluded, and a lamellar region, where rhodopsin forms nanodomains (Figure 2A). ROS disc membranes visualized by AFM represent half of a ROS disc. Nanodomains in the lamellar region were detected in a semiautomated manner and the areas of those regions were determined (Figure 2B). Various parameters of ROS disc membrane properties were measured and computed as described in the Materials and Methods.

Table 1 shows the values of parameters derived from the previous manual analysis and the current semiautomated analysis. The semiautomated detection of nanodomains resulted in the detection of a similar number of nanodomains as that from the manual method. There was a small but significant increase in the mean nanodomain size and density of rhodopsin. The distribution of nanodomain sizes is skewed.[17] Thus, the median nanodomain size was also computed since it may better reflect the average nanodomain size in a single disc membrane. Correlation analyses between various ROS disc membrane properties were also conducted as done previously.[17] All correlation analyses provided comparable results to those obtained using values derived from the manual method (Figure 3).

Table 1. Analysis of AFM Images of Wild-Type ROS Disc Membranes[a]

	parameter value		
	contact mode AFM		tapping mode AFM
ROS disc membrane properties	manual[b]	semiautomated	semiautomated
disc diameter (μm)	1.20 ± 0.25	1.22 ± 0.28	1.23 ± 0.20
inner disc area (μm^2)	0.77 ± 0.39	0.71 ± 0.34	0.75 ± 0.27
no. of nanodomains	156 ± 99	148 ± 93	151 ± 61
mean nanodomain size (nm^2)	1245 ± 379[c]	1,412 ± 403[c]	1,498 ± 344
median nanodomain size (nm^2)	997 ± 309	983 ± 275	999 ± 240
no. of rhodopsin molecules	13 513 ± 8522	14 688 ± 10 006	15 882 ± 7073
rhodopsin density (μm^{-2})	17 486 ± 6170[d]	20 420 ± 7792[d]	21 219 ± 5517

[a]AFM images of ROS disc membranes were obtained by contact mode (n = 100) or tapping mode (n = 57). Images were analyzed manually or in a semiautomated manner to obtain parameter values reported here as mean values with the associated standard deviation. [b]Values derived from manual analysis procedures were those reported previously.[17] [c]Significant difference as assessed by a two-tailed t test (p = 0.003). [d]Significant difference as assessed by a two-tailed t test (p = 0.004).

DOI: 10.1021/acs.biochem.5b00003
Biochemistry 2015, 54, 2885−2894

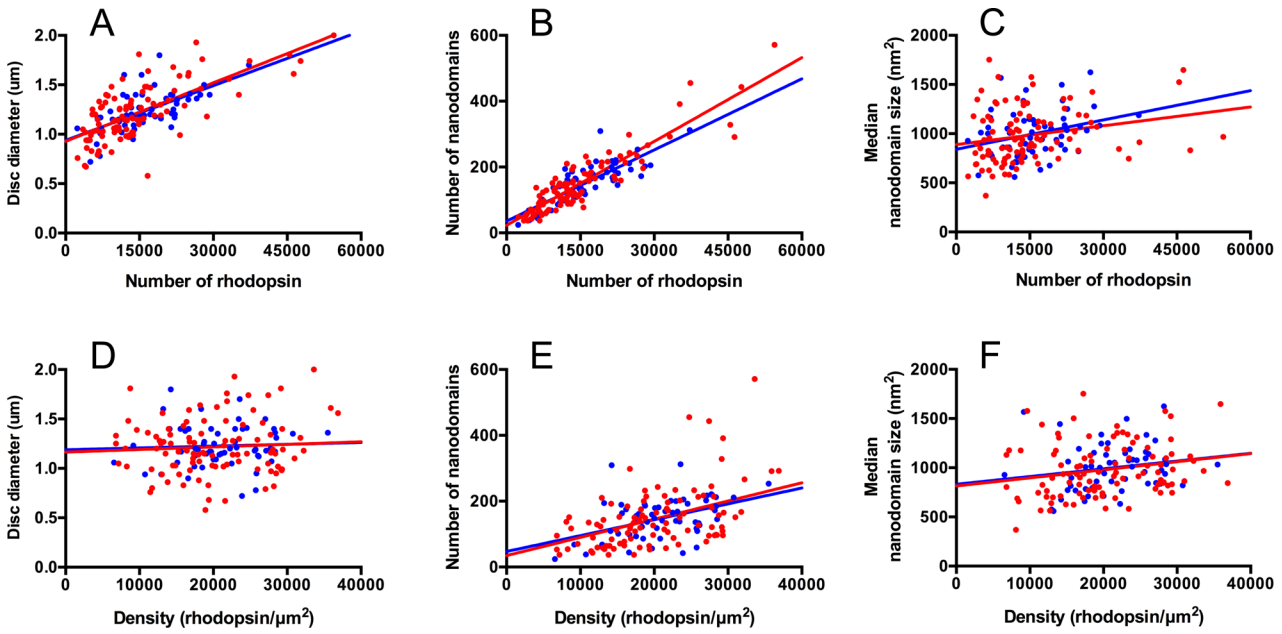

Figure 3. Correlation analyses of disc membrane properties determined from contact mode and tapping mode images. Data obtained from the analysis of contact mode images (red, $n = 100$) and tapping mode images (blue, $n = 57$) were plotted and fit by linear regression using the software Prism 6 (GraphPad Software, Inc.). A correlation analysis was conducted to compute the Pearson coefficient (r) and level of significance (p). (A) Disc diameter vs number of rhodopsin molecules. Contact mode, $r = 0.70$, $p < 0.001$. Tapping mode, $r = 0.64$, $p < 0.001$. (B) Number of nanodomains vs number of rhodopsin molecules. Contact mode, $r = 0.91$, $p < 0.001$. Tapping mode, $r = 0.83$, $p < 0.001$. (C) Median nanodomain size vs number of rhodopsin molecules. Contact mode, $r = 0.23$, $p = 0.02$. Tapping mode, $r = 0.29$, $p = 0.03$. (D) Disc diameter vs density of rhodopsin. Contact mode, $r = 0.07$, $p = 0.48$. Tapping mode, $r = 0.05$, $p = 0.71$. (E) Number of nanodomains vs density of rhodopsin. Contact mode, $r = 0.46$, $p < 0.001$. Tapping mode, $r = 0.43$, $p = 0.001$. (F) Median nanodomain size vs density of rhodopsin. Contact mode, $r = 0.23$, $p = 0.02$. Tapping mode, $r = 0.18$, $p = 0.18$.

Contact Mode versus Tapping Mode Imaging. Membrane proteins are most often imaged by either contact mode or tapping mode.[12,33,34] Previously, contact mode was used to image ROS disc membranes.[17] The nanodomains appeared to be sufficiently stable to resist deformation caused by the lateral force imparted by the AFM probe. Tapping mode is often used in imaging biological material since the AFM probe only intermittently contacts the sample, which contrasts with contact mode where the probe is in constant contact with the sample. While tapping mode is often favored in imaging biological samples due to the reduced lateral force imposed on the sample, there is a trade-off in the image acquisition time. Images can be collected much faster in contact mode compared to tapping mode in conventional AFM instruments. Thus, contact mode is preferable for obtaining a large number of images if samples are stable enough to resist deformation caused by lateral forces of the AFM probe.

To test whether contact mode alters the properties of disc membranes, AFM images were collected by tapping mode and compared with those obtained by contact mode. Tapping mode images of ROS disc membranes from 4 week old wild-type mice showed the same topography as that found in images obtained by contact mode (Figure 4). The rim region of ROS disc membranes was less disrupted and exhibited better definition in tapping mode images compared to that observed in contact mode images. The lamellar region exhibited rhodopsin organized into nanodomains of variable sizes. Nanodomains exhibited a height of 8.24 ± 1.43 nm ($n = 57$), which was similar to that observed in contact mode images.[17] AFM images obtained by tapping mode were analyzed and parameters of ROS disc membrane properties determined (Table 1). No difference was observed in any of the properties tested. Correlation analyses were also conducted to ensure that the relationships between different ROS disc membrane properties were comparable to those present in data obtained by contact mode (Figure 3). No differences were observed in any of the relationships tested. Overall, AFM images obtained by contact mode and tapping

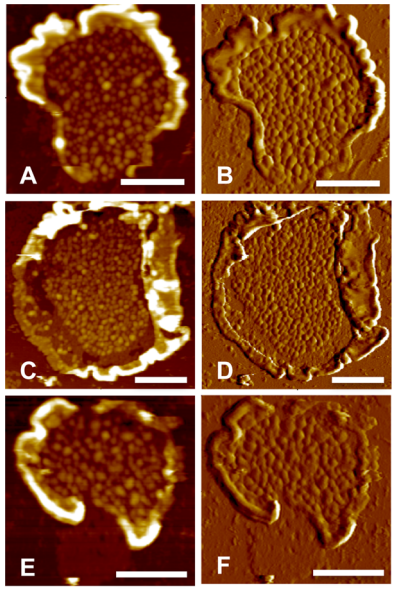

Figure 4. Tapping mode AFM images of ROS disc membranes from wild-type mice. ROS disc membranes were isolated from 4 week old wild-type mice and imaged by tapping mode AFM to obtain height (left) and amplitude (right) images. Three representative pairs of AFM images of ROS disc membranes are shown. Scale bar, 500 nm.

DOI: 10.1021/acs.biochem.5b00003
Biochemistry 2015, 54, 2885−2894

mode are comparable. Thus, contact mode images are suitable and preferable for the studies presented here.

Samples from Rho+/− Mice. Analysis of single ROS disc membranes allows for the detection of variability that exists among discs in a ROS. In wild-type mice, variability is observed in the number of rhodopsin molecules incorporated into the membrane of a single disc membrane. The number of rhodopsin molecules incorporated into the disc membrane can have significant impact on different ROS disc membrane properties (Figure 3). To determine the effect of reducing rhodopsin expression by half on ROS disc membrane properties, samples from Rho+/− mice were studied.

ROS disc membranes were obtained from 4, 6, and 8 week old Rho+/− mice and examined by AFM. Similar to samples from wild-type mice, ROS disc membranes from Rho+/− mice exhibited a rim region and lamellar region where rhodopsin forms nanodomains (Figure 5). No major differences were observed in the morphology of ROS disc membranes by visual inspection of AFM images. In contrast to deep incisures regularly observed in electron micrographs of ROS discs from Rho+/− mice,[26,27] distinct incisures were only observed in a minor population of ROS disc membranes imaged by AFM (e.g., Figure 5G and H). Thus, incisures appear to be fragile structures that can be disrupted during preparatory steps or adsorption onto the mica surface.

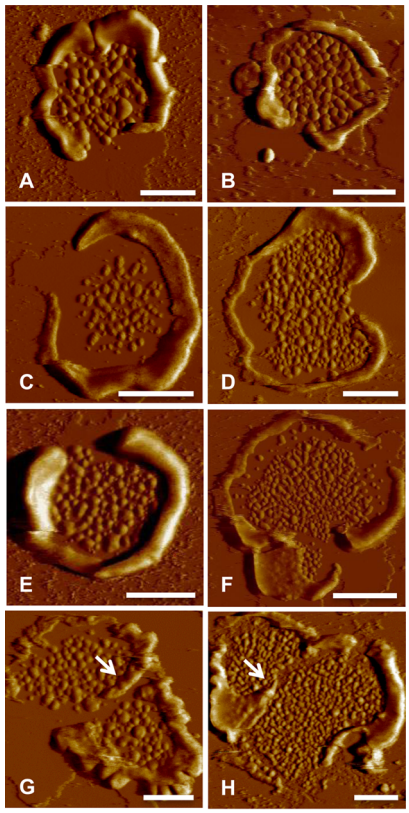

Figure 5. Contact mode AFM images of ROS disc membranes from Rho +/− mice. ROS disc membranes were isolated from 4 (A−C) and 6 (D−H) week old Rho+/− mice and imaged by contact mode AFM. Representative deflection images of ROS disc membranes are shown. The arrows point to putative incisures. Scale bar, 500 nm.

To examine in more detail the effects of reducing rhodopsin expression, ROS disc membrane properties of Rho+/− mice were quantified from AFM images (Table 2). The ROS disc membrane properties of different age groups of mice were compared to determine age-related changes (Table 3). No significant difference was observed in the sizes of disc membranes obtained from the different age groups of mice. All ROS disc membrane properties of 6 and 8 week old Rho+/− mice were similar. In contrast, significant differences were observed between most ROS disc membrane properties of 4 and 6 week old Rho+/− mice. Younger mice had less nanodomains and rhodopsin molecules incorporated into the membrane, and the densities of nanodomains and rhodopsin were also significantly lower. Both the mean and median nanodomain sizes were higher in ROS disc membranes from 4 week old mice; however, only the former was significantly different from values determined for 6 week old mice (Table 3). Taken together, the analyses revealed that significant changes in ROS disc membrane properties of Rho +/− mice occur between 4 and 6 weeks of age.

Comparison with Samples from Wild-Type Mice. Previous data collected from wild-type mice combined samples from mice that were between the ages of 4 and 6 weeks.[17] Additional AFM images of ROS disc membranes from 4, 6, and 8 week old wild-type mice were collected and analyzed to assess whether changes occur in ROS disc membranes properties during these ages (Tables 2 and 3). In contrast to Rho+/− mice, wild-type mice displayed no differences in ROS disc membrane properties among the different ages of mice tested. An exception was in the nanodomain size, where 4 week old mice had a significant increase in the mean and median nanodomain size compared to 6 week old mice. Thus, the changes observed in ROS disc membrane properties in 4 and 6 week old Rho+/− mice are specific to the reduction in rhodopsin expression except for the difference in nanodomain size.

Comparison of ROS discs membrane properties of age-matched Rho+/− and wild-type mice revealed general trends that were common across all ages of mice tested. No significant difference was observed in the size of nanodomains in ROS disc membranes obtained from age-matched Rho+/− and wild-type mice at any of the ages tested (Tables 2 and 3). The size of ROS disc membranes as assessed by disc diameter and inner disc area were smaller in Rho+/− mice compared to wild-type mice. The number of rhodopsin molecules and nanodomains present in ROS disc membranes were less in Rho+/− mice compared to wild-type mice. Some of these differences were not statistically significant (Table 3), but the overall trends were consistent across all ages tested.

Although data from all three age groups of Rho+/− mice displayed smaller values for number of rhodopsin molecules and number of nanodomains compared to age-matched wild-type mice, 4 week old mice displayed a larger decrease over age-matched wild-type mice compared to the older mice over age-matched wild-type mice (Table 2). The younger Rho+/− mice had 57% the number of rhodopsin molecules present in ROS disc membranes compared to age-matched wild-type mice, whereas 6 and 8 week old Rho+/− mice had 80% and 87%, respectively, the number of rhodopsin molecules present in ROS disc membranes compared to age-matched wild-type mice. Similarly, younger Rho+/− mice had 59% the number of nanodomains in ROS disc membranes compared to age-matched wild-type mice, whereas 6 and 8 week old Rho+/− mice had 90% and 84%, respectively, the number of nanodomains in ROS disc membranes compared to age-matched wild-type mice. A difference between 4 week old and older Rho+/− mice was also apparent in comparisons with age-matched wild-type mice for rhodopsin density and nanodomain density (Table 2). The rhodopsin and nanodomain

DOI: 10.1021/acs.biochem.5b00003
Biochemistry 2015, 54, 2885−2894

Table 2. Comparison of ROS Disc Membrane Properties of Rho+/− and Wild-Type Mice[a]

	parameter value					
	Rho+/−			wild-type		
ROS disc membrane properties	4 weeks (n = 52)	6 weeks (n = 96)	8 weeks (n = 74)	4 weeks (n = 77)	6 weeks (n = 80)	8 weeks (n = 100)
disc diameter (μm)	1.09 ± 0.25	1.14 ± 0.30	1.14 ± 0.29	1.21 ± 0.23	1.23 ± 0.31	1.22 ± 0.26
inner disc area (μm^2)	0.65 ± 0.34	0.59 ± 0.32	0.62 ± 0.34	0.71 ± 0.32	0.73 ± 0.37	0.68 ± 0.28
no. of nanodomains	86 ± 43	139 ± 103	127 ± 68	145 ± 79	154 ± 98	151 ± 71
nanodomain density (μm^{-2})	146 ± 58	234 ± 109	219 ± 76	206 ± 72	215 ± 67	227 ± 72
mean nanodomain size (nm^2)	1467 ± 355	1319 ± 429	1360 ± 289	1514 ± 368	1360 ± 389	1378 ± 449
median nanodomain size (nm^2)	988 ± 258	923 ± 332	942 ± 228	1079 ± 283	959 ± 278	911 ± 292
no. of rhodopsin molecules	8867 ± 4685	11 886 ± 7688	12 524 ± 7489	15 610 ± 9219	14 774 ± 10 200	14 404 ± 7438
rhodopsin density (μm^{-2})	14 672 ± 5489	19 853 ± 7139	20 537 ± 6080	21 654 ± 8484	20 053 ± 6188	20 979 ± 5842

[a]Parameter values reported here are mean values with the associated standard deviation. The number of AFM images of single ROS disc membranes analyzed to compute the reported values are provided (n).

Table 3. Two-Tailed t Test Results Comparing Values in Table 2

	p-value						
ROS disc membrane properties	Rho+/− 4 weeks vs Rho+/− 6 weeks	Rho+/− 6 weeks vs Rho+/− 8 weeks	wild-type 4 weeks vs wild-type 6 weeks	wild-type 6 weeks vs wild-type 8 weeks	Rho+/− 4 weeks vs wild-type 4 weeks	Rho+/− 6 weeks vs wild-type 6 weeks	Rho+/− 8 weeks vs wild-type 8 weeks
disc diameter	0.31	1.0	0.65	0.81	0.01	0.05	0.06
inner disc area	0.29	0.56	0.72	0.30	0.31	0.01	0.20
no. of nanodomains	<0.001	0.39	0.53	0.81	<0.001	0.33	0.03
nanodomain density	<0.001	0.31	0.42	0.25	<0.001	0.18	0.48
mean nanodomain size	0.04	0.48	0.01	0.78	0.47	0.51	0.76
median nanodomain size	0.22	0.67	0.01	0.26	0.07	0.44	0.45
no. of rhodopsin molecules	0.01	0.59	0.59	0.78	<0.001	0.03	0.10
rhodopsin density	<0.001	0.51	0.18	0.30	<0.001	0.84	0.63

densities were significantly lower in 4 week old Rho+/− mice compared to age-matched wild-type mice, whereas the older Rho +/− mice had similar rhodopsin and nanodomain densities compared to age-matched wild-type mice (Table 3). As suggested by comparisons of data from just the different age groups of Rho+/− mice, comparison of data from Rho+/− and wild-type mice also indicate that changes occur between 4 and 6 weeks of age in Rho+/− mice.

Correlations between disc diameter or nanodomain size and either the number of rhodopsin molecules or rhodopsin density were analyzed from data obtained from each of the age groups studied in Rho+/− and wild-type mice (Figures 6 and 7, Table 4). The correlation analyses of the three age groups of wild-type mice resulted in similar relationships as that observed in previous data that combined data from mice of different ages (Figure 3). An exception was in the correlation between nanodomain size and rhodopsin density from 4 week old mouse data, which did not show a significant correlation (Table 4). Similar to data from wild-type mice, data from Rho+/− mice exhibited a correlation between disc diameter and the number of rhodopsin molecules embedded in the disc membrane. In contrast to data from wild-type mice, data from 4 week old Rho+/− mice showed a negative correlation between disc diameter and rhodopsin density. Data from older Rho+/− mice showed an absence of correlation between these properties, which is similar to that observed with data from wild-type mice. Only data from 8 week old Rho+/− mice exhibited a correlation between nanodomain size and the number of rhodopsin molecules, which contrasts with data from wild-type mice that exhibited a correlation between these properties in all ages of mice tested. No data from Rho+/− mice exhibited a correlation between nanodomain size and rhodopsin density, whereas data from 6 and 8 week old wild-type mice showed a significant correlation in these properties. Taken together, quantitative analyses of AFM images reveal that significant differences occur in the properties of ROS disc membranes by reducing the expression of rhodopsin, some of which are age-dependent.

DISCUSSION

AFM as a Tool to Investigate ROS Disc Membrane Structure. The relationship between rhodopsin expression and ROS disc membrane structure is not fully understood. The impact of reduced rhodopsin expression on the structure of the ROS has in large part been investigated by electron microscopy.[25−27] Traditional electron microscopy approaches, however, do not provide adequate resolution to directly assess the packing of rhodopsin in the disc membrane. AFM was employed in the current study to directly assess the impact of reduced rhodopsin expression on the organization of rhodopsin within ROS disc membranes.

The survey of many individual disc membranes by AFM and the quantitative analysis of AFM images are required to assess the relationship between rhodopsin expression and ROS disc

DOI: 10.1021/acs.biochem.5b00003
Biochemistry 2015, 54, 2885−2894

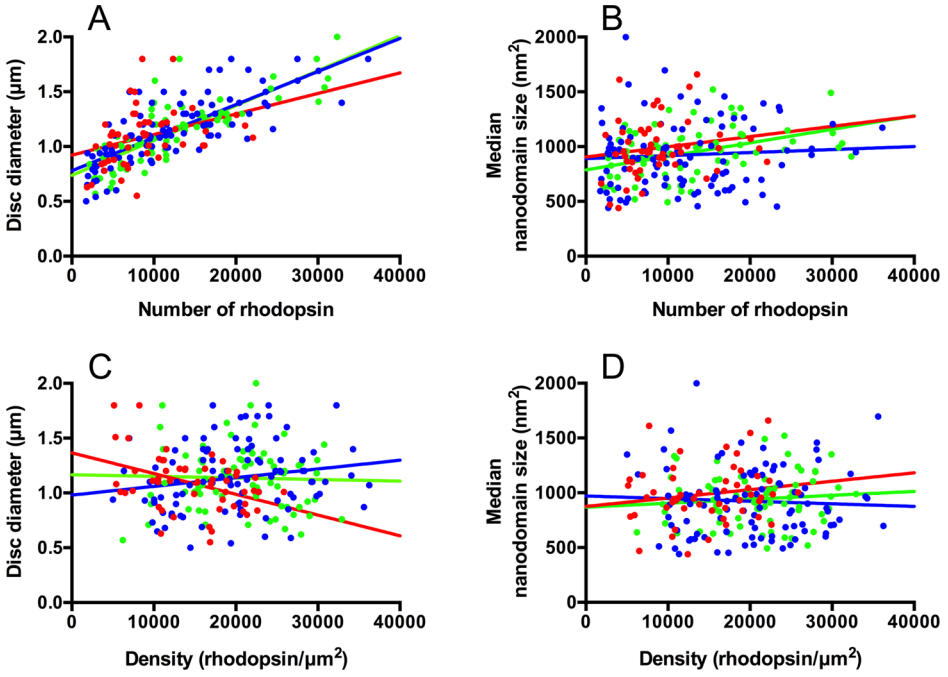

Figure 6. Correlation analyses of ROS disc membrane properties of Rho+/− mice. Data obtained from AFM images of single ROS disc membranes from 4 (red, $n = 52$), 6 (blue, $n = 96$), and 8 (green, $n = 74$) week old Rho+/− mice were plotted and fit by linear regression using the software Prism 6 (GraphPad Software, Inc.). Each data point represents data from a single ROS disc membrane, which were also used in the computation of mean values reported in Table 2. Two preparations were examined for 4 and 6 week old Rho+/− mice and one preparation was examined for 8 week old Rho+/− mice. Results of the correlation analyses conducted on these data can be found in Table 4.

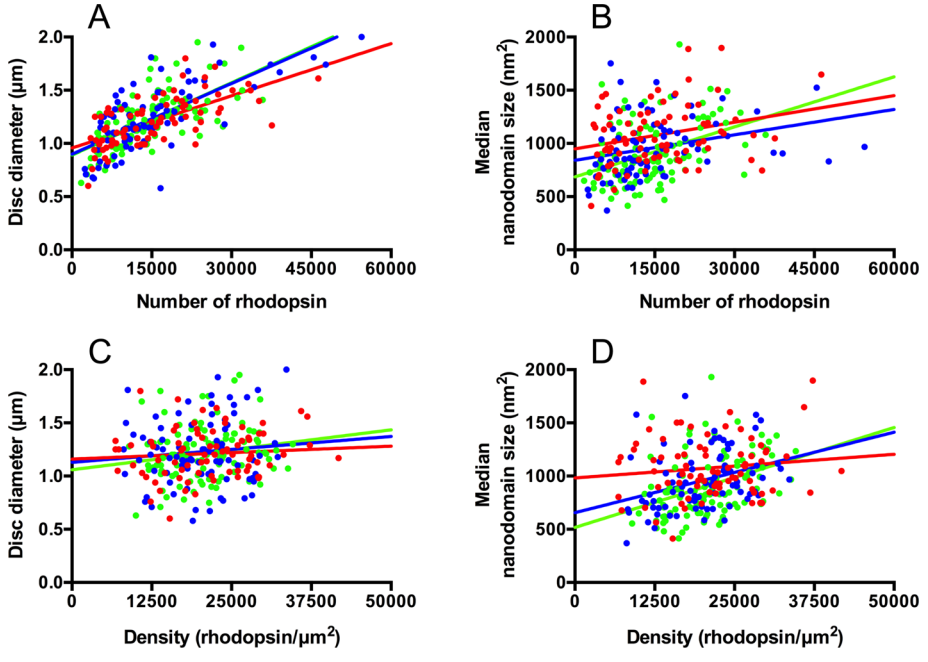

Figure 7. Correlation analyses of ROS disc membrane properties of wild-type mice. Data obtained from AFM images of single ROS disc membranes from 4 (red, $n = 77$), 6 (blue, $n = 80$), and 8 (green, $n = 100$) week old wild-type mice were plotted and fit by linear regression using the software Prism 6 (GraphPad Software, Inc.). Each data point represents data from a single ROS disc membrane, which were also used in the computation of mean values reported in Table 2. At least two preparations were examined for each age of wild-type mice. Results of the correlation analyses conducted on these data can be found in Table 4.

membrane morphology. Utilizing these methods to test a variety of experimental conditions requires the capture and analysis of a large number of AFM images. The method must be efficient and accurate. A comparison of contact mode and tapping mode images of ROS disc membranes revealed that both modes of imaging produce comparable images (Figures 2−4 and Table 1). Contact mode imaging was utilized in the current study because of faster acquisition times compared to tapping mode imaging. To make AFM practical for the quantitative studies reported in the current study, the analysis method was updated. Our previous

DOI: 10.1021/acs.biochem.5b00003
Biochemistry 2015, 54, 2885−2894

Table 4. Correlation Analysis Results[a]

correlation tested	Rho+/− 4 weeks		Rho+/− 6 weeks		Rho+/− 8 weeks		wild-type 4 weeks		wild-type 6 weeks		wild-type 8 weeks	
	r	*p*	*r*	*p*	*r*	*p*	*r*	*p*	*r*	*p*	*r*	*p*
disc diameter vs no. of rhodopsin	0.34	0.01	0.77	<0.001	0.81	<0.001	0.66	<0.001	0.72	<0.001	0.66	<0.001
disc diameter vs rhodopsin density	−0.41	0.003[b]	0.19	0.07[b]	−0.03	0.80[b]	0.09	0.44	0.10	0.40	0.17	0.09
nanodomain size vs no. of rhodopsin	0.17	0.23[c]	0.06	0.54[c]	0.41	<0.001[c]	0.27	0.02	0.29	0.01	0.40	<0.001
nanodomain size vs rhodopsin density	0.16	0.25	−0.05	0.62	0.10	0.42	0.13	0.25[d]	0.34	0.002[d]	0.38	<0.001[d]

[a]The Pearson coefficient (r) and level of significance (p) are shown for correlation analyses conducted in Figures 6 and 7. [b]The difference in the slopes of the fitted linear regression lines is significant (p = 0.005). [c]The difference in the slopes and intercepts of the fitted linear regression lines is not significant (p = 0.24 and 0.20). [d]The difference in the slopes of the fitted linear regression lines is significant (p = 0.04).

quantitative AFM study of ROS disc membranes used a manual approach to measure the size of rhodopsin nanodomains.[17] A single ROS disc membrane often contains over 100 nanodomains, and therefore, the manual measurement of each nanodomain is both time-consuming and subject to human error and bias. To improve on previous efforts, a semiautomated analysis method was implemented.

Overall, results from the semiautomated analysis method and the previous manual analysis method were comparable (Table 1). Improvements were observed in determining the size of nanodomains. Our previous manual analysis method presumed an elliptical shape for nanodomains. The semiautomatic detection of nanodomains, however, revealed that the shape of nanodomains is not purely elliptical (Figure 2B). Thus, a more accurate determination of the size of nanodomains was made possible using the semiautomated method. Improved estimates of nanodomain size resulted in a higher estimate for the density of rhodopsin (Table 1). The density value of 20 420/μm^2 computed from the semiautomated analysis method is closer to the reported estimate of 25 000/μm^2, derived from more indirect methods,[2,35] than is the value computed from the manual analysis method. Thus, the semiautomated analysis method results in improved accuracy of the data while reducing the analysis time to only a fraction of that required in the manual analysis method.

Age-Related Changes in ROS Disc Membranes from Rho+/− and Wild-Type Mice. The ROS is a dynamic structure. In wild-type mice, the ROS achieves its full adult length by postnatal day 25,[36] which corresponds to about 4 weeks of age. The increase in the length of the ROS prior to this age is achieved by changes in the rates of synthesis and phagocytosis of discs. In contrast to ROS length, the expression level of rhodopsin in the retina increases up to postnatal days 40−50, which is about 6−7 weeks of age, and remains constant thereafter.[37,38] Thus, by 4 weeks of age, the rate of disc synthesis stabilizes but the expression level of rhodopsin increases until about 6−7 weeks of age. Quantitative analyses of AFM data reveal that most ROS disc membrane properties of wild-type mice are established by 4 weeks of age (Tables 2−4), which coincides with the age at which the rate of disc synthesis stabilizes. An exception is observed in the size of nanodomains. The nanodomain size in 4 week old wild-type mice were larger than those in older mice, and no correlation was observed between nanodomain size and rhodopsin density in the younger mice, whereas a correlation was observed between these properties in older mice (Tables 2−4). Data from 4 week old Rho+/− mice also exhibited these traits. Thus, the size of nanodomains becomes established only after the expression level of rhodopsin stabilizes.

Similar to the case of wild-type mice, the size of ROS disc membranes is established in Rho+/− mice by 4 weeks of age. The reduction in rhodopsin expression results in smaller ROS disc membranes compared to those in wild-type mice, which is expected based on electron microscopy studies.[25−27] Estimates by absorption spectroscopy, Western blot, or retinoid analysis indicate that the total amount of rhodopsin in the retina of Rho +/− mice is about half of that found in the retina of wild-type mice.[6,25] At 4 weeks of age, the reduction by 43% in the number of rhodopsin molecules present in a ROS disc membrane of Rho +/− mice compared to that in wild-type mice is in good agreement with the total reduction of rhodopsin in the retina by half (Table 2).

A change occurs in Rho+/− mice, however, between 4 and 6 weeks of age, eliminating the agreement between the amount of rhodopsin in a ROS disc membrane and the total amount of rhodopsin in the retina. A 34% increase is observed in the number of rhodopsin molecules in ROS disc membranes of 6 week old Rho+/− mice compared to 4 week old Rho+/− mice (Table 2). A negative correlation between disc diameter and rhodopsin density in 4 week old Rho+/− mice that is not present in older mice or wild-type mice at any age further points to significant changes occurring in Rho+/− mice between 4 and 6 weeks of age (Figure 6C and Table 4). Thus, in wild-type mice, ROS discs appear to largely achieve their final mature state by 4 weeks of age, whereas in Rho+/− mice ROS discs continue to undergo changes until 6 weeks of age.

Maintenance of a Constant Density of Rhodopsin in ROS Disc Membranes. In wild-type mice, the density of rhodopsin in ROS disc membranes is constant across all ages of mice examined (Table 2). Thus, despite an increase in the total amount of rhodopsin in the retina occurring between 4 and 6 weeks of age,[37] a constant density of rhodopsin is maintained. In contrast, a constant density of rhodopsin is not observed across all ages of Rho+/− mice. The reduction in the number of rhodopsin molecules in ROS disc membranes of 4 week old Rho +/− mice results in a 32% decrease in the density of rhodopsin relative to that in age-matched wild-type mice (Table 2). In contrast to 4 week old mice, no significant difference was observed in the rhodopsin density of older Rho+/− mice compared to age-matched wild-type mice. Due to the smaller size of ROS disc membranes in the older Rho+/− mice relative to those in age-matched wild-type mice, less rhodopsin was required to achieve similar densities.

The observations from the current study suggest that there are mechanisms present in the ROS that maintain a constant density of rhodopsin in disc membranes, even when there is a dramatic reduction in the expression of rhodopsin as occurs in Rho+/− mice. The maintenance of a constant density of rhodopsin, however, only occurs after 4 weeks of age in the case of Rho+/−

DOI: 10.1021/acs.biochem.5b00003
Biochemistry 2015, 54, 2885−2894

mice. This regulation may occur in one or more of the stages of rhodopsin transport to the ROS and incorporation into newly formed discs (Figure 1). The mechanistic details of these events, however, are still incomplete but are actively being worked out (e.g., refs 39−46). Potential points of regulation may become apparent as clarity is achieved in these mechanistic details. The density of rhodopsin found natively in ROS disc membranes may represent the optimized density required to achieve efficient rhodopsin signaling and the sensitivity required of rod photoreceptor cells.[47] Thus, the adaptive mechanisms may be dependent on the level of signaling in the ROS. The maintenance of a constant density and organization of rhodopsin in ROS disc membranes means that previously observed changes in the electrophysiology of the ROS in Rho+/− mice are independent of these factors.[25,28]

AUTHOR INFORMATION

Corresponding Author

*Mailing address: Department of Ophthalmology and Visual Sciences, Case Western Reserve University, 2085 Adelbert Road, Room 312, Cleveland, OH 44106. Phone: 216-368-2533. Fax: 216-368-3171. E-mail: paul.park@case.edu.

Funding

This work was funded by grants from the National Institutes of Health (R01EY021731 and P30EY011373) and Research to Prevent Blindness (Unrestricted Grant and Career Development Award).

Notes

The authors declare no competing financial interest.

ACKNOWLEDGMENTS

We thank Janis Lem (Tufts Medical Center, Boston, MA) for generously providing rhodopsin knockout mice, Heather Butler and Kathryn Zongolowicz for maintaining our mouse colonies, and Ming-Jin Chang and John Denker for genotyping mice.

ABBREVIATIONS

AFM, atomic force microscopy; Rho+/−, heterozygous rhodopsin knockout; ROS, rod outer segment

REFERENCES

(1) Daemen, F. J. (1973) Vertebrate rod outer segment membranes. *Biochim. Biophys. Acta 300*, 255−288.

(2) Nickell, S., Park, P. S., Baumeister, W., and Palczewski, K. (2007) Three-dimensional architecture of murine rod outer segments determined by cryoelectron tomography. *J. Cell Biol. 177*, 917−925.

(3) Gilliam, J. C., Chang, J. T., Sandoval, I. M., Zhang, Y., Li, T., Pittler, S. J., Chiu, W., and Wensel, T. G. (2012) Three-dimensional architecture of the rod sensory cilium and its disruption in retinal neurodegeneration. *Cell 151*, 1029−1041.

(4) Young, R. W. (1967) The renewal of photoreceptor cell outer segments. *J. Cell Biol. 33*, 61−72.

(5) Papermaster, D. S., and Dreyer, W. J. (1974) Rhodopsin content in the outer segment membranes of bovine and frog retinal rods. *Biochemistry 13*, 2438−2444.

(6) Lem, J., Krasnoperova, N. V., Calvert, P. D., Kosaras, B., Cameron, D. A., Nicolo, M., Makino, C. L., and Sidman, R. L. (1999) Morphological, physiological, and biochemical changes in rhodopsin knockout mice. *Proc. Natl. Acad. Sci. U. S. A. 96*, 736−741.

(7) Humphries, M. M., Rancourt, D., Farrar, G. J., Kenna, P., Hazel, M., Bush, R. A., Sieving, P. A., Sheils, D. M., McNally, N., Creighton, P., Erven, A., Boros, A., Gulya, K., Capecchi, M. R., and Humphries, P. (1997) Retinopathy induced in mice by targeted disruption of the rhodopsin gene. *Nat. Genet. 15*, 216−219.

(8) Sung, C. H., and Chuang, J. Z. (2010) The cell biology of vision. *J. Cell Biol. 190*, 953−963.

(9) Insinna, C., and Besharse, J. C. (2008) Intraflagellar transport and the sensory outer segment of vertebrate photoreceptors. *Dev. Dyn. 237*, 1982−1992.

(10) Wang, J., and Deretic, D. (2014) Molecular complexes that direct rhodopsin transport to primary cilia. *Prog. Retinal Eye Res. 38*, 1−19.

(11) Nemet, I., Ropelewski, P., Imanishi, Y. (2015) Rhodopsin trafficking and mistrafficking: Signals, molecular components, and mechanisms. *Prog. Mol. Biol. Transl. Sci. 132*, 39−72.

(12) Whited, A. M., and Park, P. S. (2014) Atomic force microscopy: A multifaceted tool to study membrane proteins and their interactions with ligands. *Biochim. Biophys. Acta 1838*, 56−68.

(13) Muller, D. J. (2008) AFM: A nanotool in membrane biology. *Biochemistry 47*, 7986−7998.

(14) Engel, A., and Gaub, H. E. (2008) Structure and mechanics of membrane proteins. *Annu. Rev. Biochem. 77*, 127−148.

(15) Buzhynskyy, N., Salesse, C., and Scheuring, S. (2011) Rhodopsin is spatially heterogeneously distributed in rod outer segment disk membranes. *J. Mol. Recognit. 24*, 483−489.

(16) Liang, Y., Fotiadis, D., Filipek, S., Saperstein, D. A., Palczewski, K., and Engel, A. (2003) Organization of the G protein-coupled receptors rhodopsin and opsin in native membranes. *J. Biol. Chem. 278*, 21655−21662.

(17) Whited, A. M., and Park, P. S. (2015) Nanodomain organization of rhodopsin in native human and murine rod outer segment disc membranes. *Biochim. Biophys. Acta 1848*, 26−34.

(18) Gunkel, M., Schoneberg, J., Alkhaldi, W., Irsen, S., Noe, F., Kaupp, U. B., and Al-Amoudi, A. (2015) Higher-order architecture of rhodopsin in intact photoreceptors and its implication for phototransduction kinetics. *Structure 23*, 628−638.

(19) Dell'Orco, D. (2013) A physiological role for the supramolecular organization of rhodopsin and transducin in rod photoreceptors. *FEBS Lett. 587*, 2060−2066.

(20) Hartong, D. T., Berson, E. L., and Dryja, T. P. (2006) Retinitis pigmentosa. *Lancet 368*, 1795−1809.

(21) Daiger, S. P., Sullivan, L. S., and Bowne, S. J. (2013) Genes and mutations causing retinitis pigmentosa. *Clin. Genet. 84*, 132−141.

(22) Mendes, H. F., van der Spuy, J., Chapple, J. P., and Cheetham, M. E. (2005) Mechanisms of cell death in rhodopsin retinitis pigmentosa: implications for therapy. *Trends Mol. Med. 11*, 177−185.

(23) Sung, C. H., Davenport, C. M., and Nathans, J. (1993) Rhodopsin mutations responsible for autosomal dominant retinitis pigmentosa. Clustering of functional classes along the polypeptide chain. *J. Biol. Chem. 268*, 26645−26649.

(24) Krebs, M. P., Holden, D. C., Joshi, P., Clark, C. L., 3rd, Lee, A. H., and Kaushal, S. (2010) Molecular mechanisms of rhodopsin retinitis pigmentosa and the efficacy of pharmacological rescue. *J. Mol. Biol. 395*, 1063−1078.

(25) Liang, Y., Fotiadis, D., Maeda, T., Maeda, A., Modzelewska, A., Filipek, S., Saperstein, D. A., Engel, A., and Palczewski, K. (2004) Rhodopsin signaling and organization in heterozygote rhodopsin knockout mice. *J. Biol. Chem. 279*, 48189−48196.

(26) Makino, C. L., Wen, X. H., Michaud, N. A., Covington, H. I., DiBenedetto, E., Hamm, H. E., Lem, J., and Caruso, G. (2012) Rhodopsin expression level affects rod outer segment morphology and photoresponse kinetics. *PLoS One 7*, e37832.

(27) Price, B. A., Sandoval, I. M., Chan, F., Nichols, R., Roman-Sanchez, R., Wensel, T. G., and Wilson, J. H. (2012) Rhodopsin gene expression determines rod outer segment size and rod cell resistance to a dominant-negative neurodegeneration mutant. *PLoS One 7*, e49889.

(28) Calvert, P. D., Govardovskii, V. I., Krasnoperova, N., Anderson, R. E., Lem, J., and Makino, C. L. (2001) Membrane protein diffusion sets the speed of rod phototransduction. *Nature 411*, 90−94.

(29) Park, P. S., Sapra, K. T., Jastrzebska, B., Maeda, T., Maeda, A., Pulawski, W., Kono, M., Lem, J., Crouch, R. K., Filipek, S., Muller, D. J., and Palczewski, K. (2009) Modulation of molecular interactions and function by rhodopsin palmitylation. *Biochemistry 48*, 4294−4304.

DOI: 10.1021/acs.biochem.5b00003
Biochemistry 2015, 54, 2885−2894

(30) Hansma, H. G., and Hoh, J. H. (1994) Biomolecular imaging with the atomic force microscope. *Annu. Rev. Biophys. Biomol. Struct. 23*, 115−139.
(31) Frederix, P. T., Hoogenboom, B. W., Fotiadis, D., Muller, D. J., and Engel, A. (2004) Atomic force microscopy of biological samples. *MRS Bull. 29*, 449−455.
(32) Park, P. S., and Muller, D. J. (2015) Dynamic single-molecule force spectroscopy of rhodopsin in native membranes. *Methods Mol. Biol. 1271*, 173−185.
(33) Binnig, G., Quate, C. F., and Gerber, C. (1986) Atomic force microscope. *Phys. Rev. Lett. 56*, 930−933.
(34) Zhong, Q., Inniss, D., Kjoller, K., and Elings, V. B. (1993) Fractured Polymer Silica Fiber Surface Studied by Tapping Mode Atomic-Force Microscopy. *Surf. Sci. 290*, L688−L692.
(35) Liebman, P. A., Parker, K. R., and Dratz, E. A. (1987) The molecular mechanism of visual excitation and its relation to the structure and composition of the rod outer segment. *Annu. Rev. Physiol. 49*, 765−791.
(36) LaVail, M. M. (1973) Kinetics of rod outer segment renewal in the developing mouse retina. *J. Cell Biol. 58*, 650−661.
(37) Carter-Dawson, L., Alvarez, R. A., Fong, S. L., Liou, G. I., Sperling, H. G., and Bridges, C. D. (1986) Rhodopsin, 11-cis vitamin A, and interstitial retinol-binding protein (IRBP) during retinal development in normal and rd mutant mice. *Dev. Biol. 116*, 431−438.
(38) Sakami, S., Kolesnikov, A. V., Kefalov, V. J., and Palczewski, K. (2014) P23H opsin knock-in mice reveal a novel step in retinal rod disc morphogenesis. *Hum. Mol. Genet. 23*, 1723−1741.
(39) Wang, J., Morita, Y., Mazelova, J., and Deretic, D. (2012) The Arf GAP ASAP1 provides a platform to regulate Arf4- and Rab11-Rab8-mediated ciliary receptor targeting. *EMBO J. 31*, 4057−4071.
(40) Bhowmick, R., Li, M., Sun, J., Baker, S. A., Insinna, C., and Besharse, J. C. (2009) Photoreceptor IFT complexes containing chaperones, guanylyl cyclase 1 and rhodopsin. *Traffic 10*, 648−663.
(41) Chuang, J. Z., Hsu, Y. C., and Sung, C. H. (2015) Ultrastructural visualization of trans-ciliary rhodopsin cargoes in mammalian rods. *Cilia 4*, 4.
(42) Lodowski, K. H., Lee, R., Ropelewski, P., Nemet, I., Tian, G., and Imanishi, Y. (2013) Signals governing the trafficking and mistrafficking of a ciliary GPCR, rhodopsin. *J. Neurosci. 33*, 13621−13638.
(43) Reish, N. J., Boitet, E. R., Bales, K. L., and Gross, A. K. (2014) Nucleotide bound to rab11a controls localization in rod cells but not interaction with rhodopsin. *J. Neurosci. 34*, 14854−14863.
(44) Crouse, J. A., Lopes, V. S., Sanagustin, J. T., Keady, B. T., Williams, D. S., and Pazour, G. J. (2014) Distinct functions for IFT140 and IFT20 in opsin transport. *Cytoskeleton 71*, 302−310.
(45) Trivedi, D., Colin, E., Louie, C. M., and Williams, D. S. (2012) Live-cell imaging evidence for the ciliary transport of rod photoreceptor opsin by heterotrimeric kinesin-2. *J. Neurosci. 32*, 10587−10593.
(46) Hsu, Y. C., Chuang, J. Z., and Sung, C. H. (2015) Light regulates the ciliary protein transport and outer segment disc renewal of Mammalian photoreceptors. *Dev. Cell 32*, 731−742.
(47) Saxton, M. J., and Owicki, J. C. (1989) Concentration effects on reactions in membranes: rhodopsin and transducin. *Biochim. Biophys. Acta 979*, 27−34.

DOI: 10.1021/acs.biochem.5b00003
Biochemistry 2015, 54, 2885−2894